Ferrite $Sr_3NdFe_3O_9$: An Original Intergrowth between the Brownmillerite and K_2NiF_4-type Structures

N. Barrier,[†] D. Pelloquin,*[,†] N. Nguyen,[†] M. Giot,[‡] F. Bourée,[‡] and B. Raveau[†]

Laboratoire de Cristallographie et Sciences des Materiaux, Unité Mixte de Recherche 6508 Centre National de la Recherche Scientifique, Institut des Sciences de la Materière et du Rayonnement, 6 boulevard Maréchal Juin, 14050 Caen Cedex 4, France, and Laboratoire Léon Brillouin, Commissariat à l'Energie Atomique de Saclay, 91191 Gif-sur-Yvette Cedex, France

Received August 3, 2005. Revised Manuscript Received September 27, 2005

The coupled neutron diffraction and Mossbaüer study of the layered oxide $Sr_3NdFe_3O_9$ shows for the first time the possibility of anionic vacancies ordering in an oxygen-deficient related Ruddlesden−Popper- (RP-) type ferrite leading to an original intergrowth of brownmillerite and K_2NiF_4-type layers. The antiferromagnetic properties of this phase up to 500 K are also evidenced. These results open the route to the synthesis of new members in the series $(Sr_2Fe_2O_5)_n$·$SrLnFeO_4$ and to the understanding of their reactivity with atmospheric water.

Introduction

Since the discovery of layered related perovskite compounds in the Sr−Ti−O system by Ruddlesden and Popper,[1] many studies have been carried out to discover other layered structures built up from the intergrowth of rock salt layers with single or multiple perovskite layers. The numerous results obtained about the high-T_c superconducting layered cuprates[2] have shown that such oxides exhibit, besides the intergrowth phenomena, a large oxygen deficiency involving an ordering of the oxygen atoms and anionic vacancies. The latter phenomena were explained by the Jahn−Teller effect of copper, which induces a pyramidal or square planar coordination of copper. In contrast, in the layered manganites, the Ruddlesden−Popper (RP) phases tend to be stoichiometric, so that no particular ordering of oxygen atoms and vacancies was detected despite the ability of Mn^{3+} to exhibit the Jahn−Teller effect.

In this respect, the layered ferrites are of great interest since several RP derivatives have also been obtained where the distorted octahedral coordination of iron can better be described as a 5 + 1 pyramidal environment, as shown for example in thallium and lead ferrites (for a review see ref 3). Moreover, the possibility of oxygen deficiency[4] and of water molecule intercalation[5] was recently demonstrated in the RP phase $Sr_3LaFe_3O_{10-\delta}$. More recently, we showed that the oxygen-deficient RP phase $Sr_3NdFe_3O_9$ reacts topotactically with ambient moisture to form a new series of hydrated oxyhydroxides closely related to the RP-type structures.[6]

To understand the mechanism of this topotactic reaction in the oxygen-deficient $Sr_3LnFe_3O_9$, the accurate determination of the crystal structure was absolutely necessary, especially to locate the oxygen vacancies. We report herein on the neutron diffraction study of the latter phase and we show for the first time that iron-based related RP phases exhibit an ordered oxygen deficiency, forming brownmillerite layers intergrown with rock salt layers. An antiferromagnetic behavior of $Sr_3NdFe_3O_9$ up to 500 K is also shown.

Experimental Section

The $Sr_3NdFe_3O_9$ oxide was synthesized by a solid-state route according to the same experimental conditions as previously reported.[6] About 5 g of sample has been prepared starting from adequate mixtures of SrO_2, Nd_2O_3, Fe_2O_3 oxides, and Fe metal. The samples were first intimately ground in an agate mortar and then pressed in the form of bars. They were placed in evacuated quartz tubes and heated to 1200 °C with a heating rate of 200 °C·h^{-1}, held at this temperature for 24 h, and cooled to room temperature in 12 h. To avoid the reaction with ambient moisture and the formation of the hydrated derivative $Sr_3NdFe_3O_{7.5}(OH)_2$·H_2O,[6] the tubes were broken just before the experiments.

The high-resolution electron microscopy (HREM) images were recorded with a JEOL 2011 FEG microscope operating at 200 kV and equipped with an energy-dispersive spectroscopy (EDS) analyzer.

X-ray powder diffraction patterns were collected on a Philips X'pertPro diffractometer equipped with an X'Celerator detector working with Cu Kα radiation. This system is equipped with an Anton Paar TTK450 chamber allowing data collection at room temperature, by step scanning over an angular range $4° \leq 2\theta \leq 120°$, under dynamic vacuum. Neutron powder diffraction data were recorded on the high-resolution diffractometer 3T2 ($\lambda = 1.225$ Å) at the Orphée reactor of the Laboratoire Léon Brillouin (CEA/Saclay). Data collections were performed at room temperature and at 673 K and were then treated by profile analysis with the Jana 2000 program.[7]

* Corresponding author: e-mail denis.pelloquin@ensicaen.fr.
† Laboratoire CRISMAT, UMR 6508 CNRS ISMRA.
‡ Laboratoire Léon Brillouin-CEA-Saclay.

(1) (a) Ruddlesden, S. N.; Popper, P. *Acta Crystallogr.* **1957**, *10*, 538. (b) Ruddlesden, S. N.; Popper, P. *Acta Crystallogr.* **1958**, *11*, 54.
(2) Raveau, B.; Michel, C.; Hervieu, M.; Groult, D. *Crystal Chemistry of High TC superconducting copper oxide*; Springer-Verlag: Berlin, 1991.
(3) Raveau, B.; Hervieu, M.; Pelloquin, D.; Michel, C.; Retoux, R. *Z. Anorg. Chem.* **2005**, *631*, 1831.
(4) Lee, J. Y.; Swinnea, J. S.; Steinfink, H.; Reiff, W. M.; Pei, S.; Jorgensen, J. D. *J. Solid State Chem.* **1993**, *103*, 1.
(5) Nishi, T.; Toda, K.; Kanamaru, F.; Sakai, T. *Key Eng. Mater.* **1999**, *169−170*, 235.
(6) Pelloquin, D.; Hadermann, J.; Giot, M.; Caignaert, V.; Michel, C.; Hervieu, M.; Raveau, B. *Chem. Mater.* **2004**, *16*, 1715.

10.1021/cm051729f CCC: $30.25
Published on Web 11/30/2005

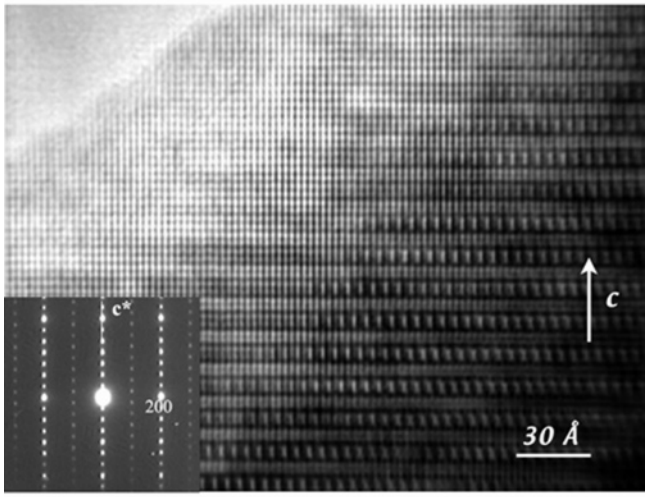

Figure 1. Experimental [010] HREM image recorded with a defocus value of −150 Å and corresponding ED pattern (inset).

The powder Mössbauer resonance spectra were measured at room temperature in a transmission geometry by use of a constant-acceleration spectrometer and a ^{57}Co source diffused into a rhodium matrix. The velocity scale was calibrated with an α-Fe foil at room temperature. The spectra were fitted with Lorentzian lines by the unpublished MOSFIT program. The isomer shift values are given with respect to metallic iron at 293 K.

The magnetic properties were studied by use of a Faraday balance (0.3 T; from room temperature to 650 K).

Results and Discussion

Evidence for Antiferromagnetic Behavior at Room Temperature. First, the purity of the sample was checked at 300 K from X-ray powder diffraction data analysis; this revealed some amount of $SrNdFeO_4$ oxide[8] as a secondary phase. The diffraction peak positions of the main phase $Sr_3NdFe_3O_9$ evidenced a distorted orthorhombic lattice[6] with regard to the ideal *I*-type tetragonal ($a_p \times a_p \times 28$ Å^3) $n = 3$ RP structure. This distortion was confirmed by transmission electron microscopy since the electron diffraction patterns analysis revealed a supercell ($a_p\sqrt{2} \times a_p \sqrt{2} \times 28$ Å^3) crystallizing in the *Bbmm* or *Bbm*2 space group. In the same way, EDS analysis carried out on numerous crystallites confirmed the homogeneity of the as-prepared sample with an actual cationic composition close to Sr_3NdFe_3, in agreement with the starting composition. The origin of this structural distortion was scanned from HREM images, especially along the [010] direction for which the superstructure is clearly visible on the ED pattern. An ordered contrast is indeed observed at the level of the perovskite block, as illustrated in Figure 1. From this image, recorded with a defocus value close to −150 Å for which the low electron density zones are correlated to the bright dots, the $a_p\sqrt{2}$ periodicity along $\vec{a}$ results from alternating bright and less bright spots, while along $\vec{c}$, this sequence between two successive perovskite blocks is shifted by ∼2.76Å in agreement with the *B*-type symmetry.

Second, the magnetic behavior of this layered ferrite was studied across a large temperature range, from 300 to 673 K. The magnetization measurements evidence antiferromagnetic interactions at room temperature while the paramagnetic state is reached only at $T \approx 600$ K (Figure 2). Note that the $SrNdFeO_4$ oxide, detected as a secondary phase, is well-known to exhibit antiferromagnetic interactions below 270 K.[9] This behavior is corroborated by neutron diffraction data collected at room temperature (rt) and at 673 K, which evidence only some extra magnetic peaks at RT. It can be also compared to that reported for the $Sr_3LaFe_3O_{10-\delta}$ ($0.1 < \delta < 0.8$) series,[4] where ferromagnetic and antiferromagnetic exchange interactions were observed below 200 K, the first one for small values of δ and the second one for large values. Moreover, as reported previously,[6] the aforementioned $Sr_3NdFe_3O_9$ oxide is very sensitive to ambient moisture, forming a hydrated $Sr_3NdFe_3O_{7.5}(OH)_2,H_2O$ oxyhydroxide. This reactivity is correlated to a large oxygen deficiency compared to the theoretical "O_{10}" stoichiometry expected for an ideal $n = 3$ RP-type structure. Such observations should be ascribed to an oxygen/vacancy ordering as in the brownmillerite derivatives. To validate this interpretation and to discuss the formation of the hydrated $Sr_3NdFe_3O_{7.5}(OH)_2,H_2O$ oxyhydroxide, a neutron diffraction study has been carried out on the as-prepared $Sr_3NdFe_3O_9$ oxide from data collected at $T = 673$ K to avoid the presence of magnetic diffraction peaks.

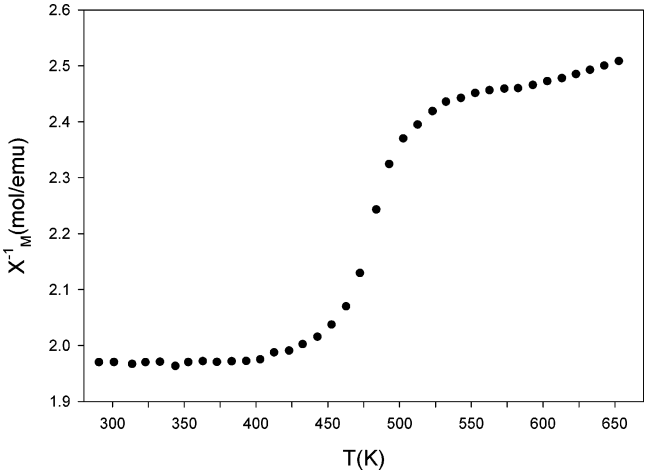

Figure 2. Inverse susceptibility (χ^{-1}) versus temperature (T) data ranging from room temperature to 650 K.

Neutron Diffraction Study. Rietveld refinements were first carried out with the atomic positions of the previous X-ray diffraction study[6] in the *Bbm*2 space group. Nevertheless, the relatively high *R* factors indicated that some atomic positions were wrong as well as the variations of most *z* atomic coordinates, indicating that the higher symmetry *Bbmm* space group should better describe the structure.

Then the crystal structure determination was made with the assumption of the *Bbmm* space group with the parameters $a = 5.5414(9)$ Å, $b = 5.4986(9)$ Å, and $c = 28.810(5)$ Å. The observed intensities were extracted from the neutron data by the Jana2000 program,[7] and the atomic positions were determined by direct methods with the EXPO program.[10] Two Sr/Nd and two Fe sites were located as predicted by X-ray diffraction as well as five O anion positions, giving a

(7) Petricek, V.; Dusek, M. JANA 2000 software, Institute of Physics, Academy of Science of the Czech Republik, Prague.
(8) Joubert, J. C.; Collomb, A.; Elmaleh, D.; Le Flem, G.; Daoudi, A.; Ollivier, G. J. *J. Solid State Chem.* **1970**, *2*, 343.
(9) Shimada, M.; Korizumi, M. *Mater. Res. Bull.* **1976**, *11* (10), *1237*.

Table 1. Conditions of Neutron Data Collection and Agreement Factors for $Sr_3NdFe_3O_9$

diffractometer	3T2 (LLB)
radiation type	neutron, $\lambda = 1.2252$ Å
angular range (2θ, deg)	6.00−125.70
step scan increment (2θ, deg)	0.05
temperature (K)	673
no. of points	2395
total no. of refined parameters	66
no.of reflections	941
profile function	Thompson−Cox−Hasting pseudo-Voigt
background function	manual
preferred orientation	March and Dollase
R_p	0.0381
R_{wp}	0.1164
R_{exp}	0.1029

phases	$Sr_3NdFe_3O_9$	$SrNdFeO_4$
no. of refined crystallographic parameters	50	2 (cell parameters)
R_{obs}	0.0320	0.0369
R_w	0.0301	0.0287

consistent formula: $Sr_3NdFe_3O_9$. The structure *R* factor of 6.74% obtained from the refinement of this model confirms the choice of the novel space group and the validity of the atomic positions except for the O5 atom on a 4c (x, $^1/_4$, 0) position that presented a huge U_{iso} atomic displacement parameter (ADP) of 0.36(10). This oxygen atom was then split between 8g (x, y, 0) positions with the assumption of 50% site occupancy, and the refined U_{iso} ADP became equal to 0.061(8). This delocalization of the oxygen atoms within the tetrahedral sheet parallel to the (*ab*) plane is also observed in the $Ba_2In_2O_5$ brownmillerite-type compound.[11] At this time some diffraction peaks were not indexed and were identified as belonging to the $SrNdFeO_4$[8] phases. The crystallographic parameters of these two extra phases were introduced in our model and the unit-cell parameters were refined as well as their relative scale factors. The amounts in mass of $Sr_3NdFe_3O_9$ and $SrNdFeO_4$ are 0.896(4) and 0.104(4), respectively. At the end, anisotropic ADPs were assumed except for the O5 atom and all oxygen sites were checked to be fully occupied, leading to the stoichiometric formula $Sr_3NdFe_3O_9$. The final profile and structure *R* factors with all refinement conditions are given in Table 1; the crystallographic parameters and selected interatomic distances are reported in Tables 2 and 3, respectively. The neutron powder diffraction pattern of this phase is shown in Figure 3.

The crystal structure of $Sr_3NdFe_3O_9$ (Figure 4) can be described as an intergrowth of a brownmillerite-type layer, $Sr_2Fe_2O_5$, with a K_2NiF_4-type layer, $SrNdFeO_4$, along the *c* axis. The resulting $[Fe_3O_9]^{9-}$ framework is built of a central sheet of parallel chains of FeO_4 tetrahedra and parallel rows of oxygen vacancies running along *b*. By this way, this compound can be considered as an ordered oxygen-deficient $n = 3$ RP phase with the formula $Sr_3NdFe_3O_9\square$, where $\square$ represents the oxygen vacancy. This tetrahedral sheet is sandwiched between two octahedral FeO_3 perovskite-like sheets. All the octahedra share one apex oxygen atom with tetrahedra of the central sheet. Along the *c* axis, two successive $[Fe_3O_9]^{9-}$ blocks are shifted by $(\vec{a}_p + \vec{b}_p)/2$ as observed in the $n = 3$ RP phases. In the same way we observe the shifting by *a*/2 for the oxygen vacancy rows between two successive blocks along the *c* axis in agreement with the ordered contrast on the HREM image along the [010] direction (Figure 1).

Because of the short O5−O5 distance (1.35(5) Å), two adjacent O5 atomic sites cannot be simultaneously occupied. The distribution of these oxygen atoms is shown in Figure 5 as well as the two limit distributions leading to tetrahedral sheets similar to those observed in the brownmillerite-type compounds. The chains running along the *b* axis are formed by distorted FeO_4 tetrahedra that share one oxygen atom and present three short Fe2−O bonds ranging from 1.754 to 1.882 Å and a long Fe2−O5 distance of 2.110 Å. Within the two other iron sheets, the FeO_6 octahedra are strongly distorted along the *c* axis with a long Fe1−O4 distance of 2.513 Å against five shorter Fe1−O distances ranging from 1.961 to 1.991 Å. From this point of view, the Fe1 atom environment can be considered as 5 + 1 coordination, intermediate between an FeO_5 square base pyramid and an FeO_6 octahedron. This distortion along the *c* axis allows the tilting of the FeO_6 octahedra to be significantly decreased with respect to that usually observed in the brownmillerite-type com-

Table 2. Crystallographic Parameters for $Sr_3NdFe_3O_9$

Crystal Data

formula sum	$Sr_3Nd_1O_9Fe_3$
crystal system	orthorhombic
space group	*Bbmm* (no. 63)
unit cell dimensions	
a, Å	5.5414(9)
b, Å	5.4986(9)
c, Å	28.810(5)
cell volume, Å^3	877.8(4)
Z	4

Atomic Coordinates and Isotropic Equivalent Displacement Parameters (Å^2)

atom	occ.	x	y	z	U_{iso} equiv
Fe1		0.2507(19)	0.750 00	0.1447(2)	0.0169(16)
Fe2		0.306(3)	0.750 00	0.000 00	0.053(5)
Sr1/Nd1	0.75/0.25	−0.252(3)	0.750 00	0.2030(2)	0.019(2)
Sr2/Nd2	0.75/0.25	−0.241(3)	0.750 00	0.0787(3)	0.021(3)
O1		0.000 00	0.500 00	0.1393(5)	0.024(4)
O2		0.500 00	0.000 00	0.1356(6)	0.027(5)
O3		0.257(4)	0.750 00	0.2138(3)	0.032(3)
O4		0.212(5)	0.750 00	0.0578(4)	0.075(8)
O5	0.5	0.377(5)	0.127(6)	0.000 00	0.061(8)

Anisotropic Displacement Parameters (Å^2)

atom	U_{11}	U_{22}	U_{33}	U_{12}	U_{13}	U_{23}
Fe1	0.013(3)	0.011(2)	0.027(3)	0.000 00	−0.012(4)	0.000 00
Fe2	0.050(11)	0.092(12)	0.017(4)	0.000 00	0.000 00	0.000 00
Sr1	0.028(4)	0.020(4)	0.009(3)	0.000 00	−0.011(6)	0.000 00
Sr2	0.024(5)	0.018(4)	0.021(4)	0.000 00	−0.010(6)	0.000 00
O1	0.026(7)	0.027(9)	0.018(6)	−0.020(5)	0.000 00	0.000 00
O2	0.020(7)	0.011(10)	0.050(9)	0.017(5)	0.000 00	0.000 00
O3	0.046(7)	0.032(5)	0.018(4)	0.000 00	0.000(11)	0.000 00
O4	0.088(17)	0.094(15)	0.043(7)	0.000 00	0.034(11)	0.000 00

Table 3. Interatomic Bond Distances[a] in $Sr_3NdFe_3O_9$

Fe1	O1	1.961(8)	2×	Fe2	O4	1.745(15)	2×
Fe1	O2	1.966(8)	2×	Fe2	O5	1.882(32)	2×
Fe1	O3	1.991(10)	1×	Fe2	O5	2.110(33)	2×
Fe1	O4	2.513(13)	1×	Sr2	O5	2.483(15)	2×
Sr1	O3	2.397(10)	1×	Sr2	O2	2.576(15)	2×
Sr1	O1	2.685(14)	2×	Sr2	O4	2.581(32)	1×
Sr1	O3	2.739(28)	1×	Sr2	O1	2.593(14)	2×
Sr1	O2	2.748(15)	2×	Sr2	O4	2.819(4)	2×
Sr1	O3	2.767(1)	2×	O5	O5	1.353(47)	1×
Sr1	O3	2.838(28)	1×	O5	O5	1.952(43)	1×

[a] Bond distances are given in angstroms.

(10) Altomare, A.; Burla, M. C.; Camalli, M.; Carrozzini, B.; Cascarano, G.; Giacovazzo, C.; Guagliardi, A.; Moliterni, A. G. G.; Polidori, G.; Rizzi, R. EXPO: a program for full powder pattern decomposition and crystal structure solution. *J. Appl. Crystallogr.* **1998**, *32*, 339.

(11) Berastegui, P.; Hull, S.; Garcia-Garcia, F. J.; Eriksson, S. G. *J. Solid State Chem.* **2002**, *164*, 119.

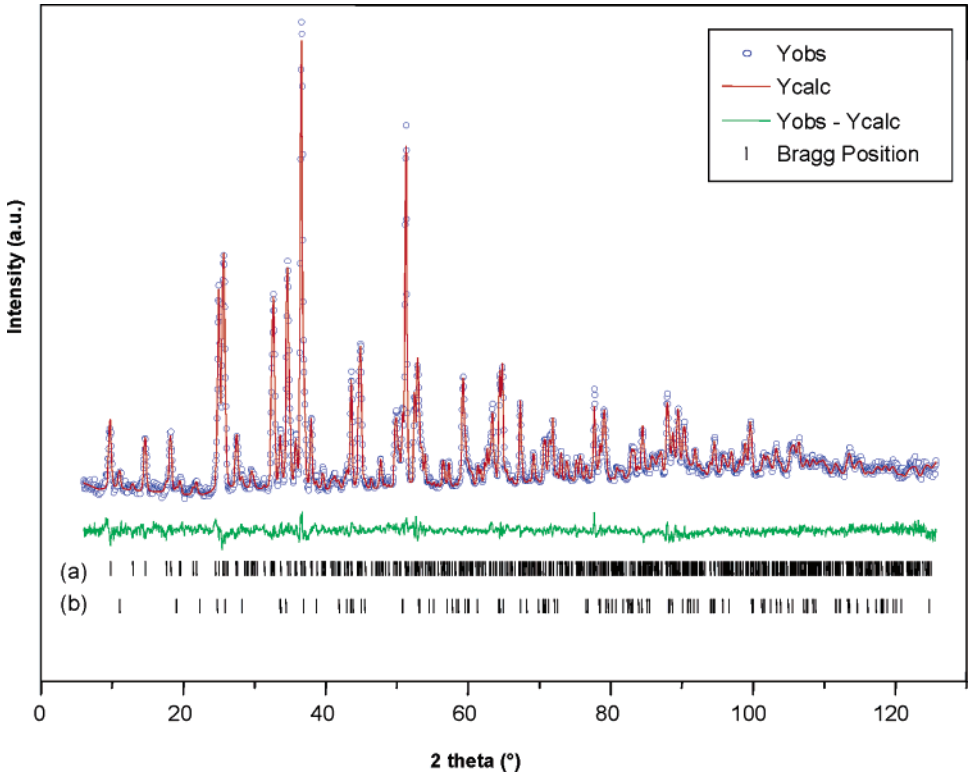

Figure 3. Neutron powder diffraction pattern recorded at 673 K (λ = 1.2252 Å) with observed (symbols) and calculated (lines) profiles and below the difference curve. Tick marks represent the Bragg reflections of $Sr_3NdFe_3O_9$ (a) and $SrNdFeO_4$ (b).

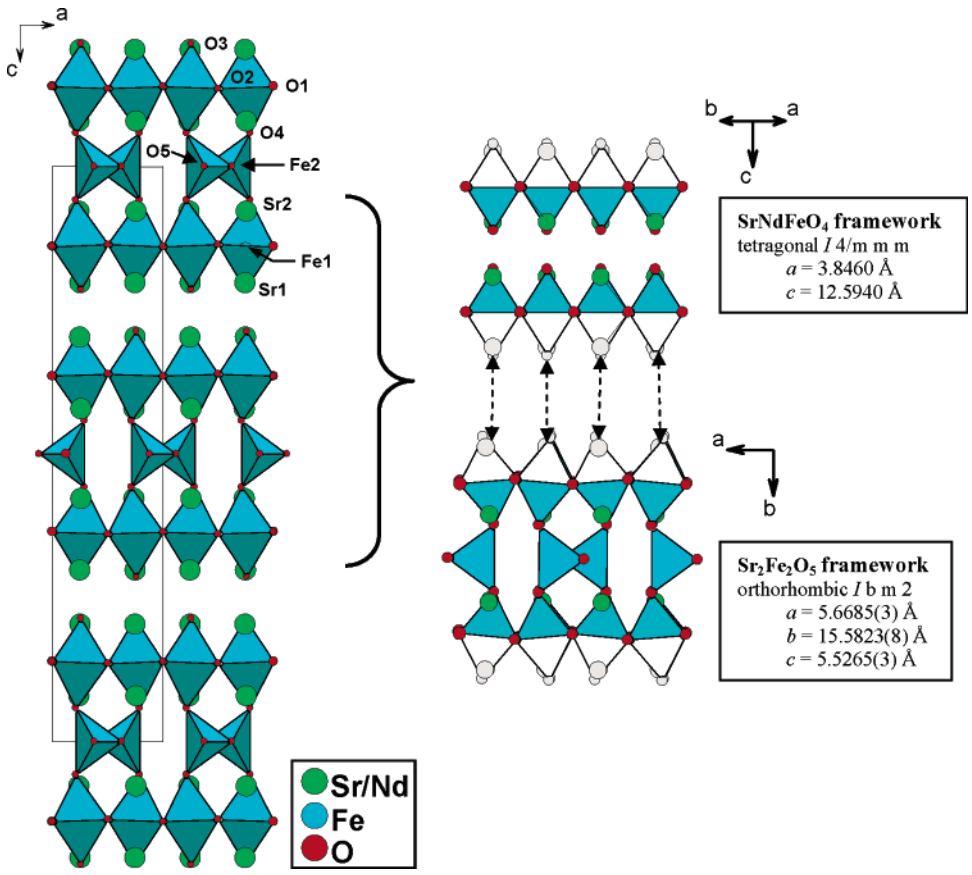

Figure 4. Crystal structure of $Sr_3NdFe_3O_9$ (left) resulting in the intergrowth of a brownmillerite-type layer, $Sr_2Fe_2O_5$, with a K_2NiF_4-type layer, $SrNdFeO_4$, along the *c* axis.

pounds. The angle between two adjacent octahedra along the *a* direction is indeed 175.5° against 170.2° and 162.3° in the brownmillerite-type compounds $Ba_2In_2O_5$[11] and Ca_2AlFeO_5,[13] respectively. Bond valence calculation (Table 4)[14] for the two Fe1 and Fe2 atom types leads to the respective values of +3.18(8) and +2.97(3), close to the expected value

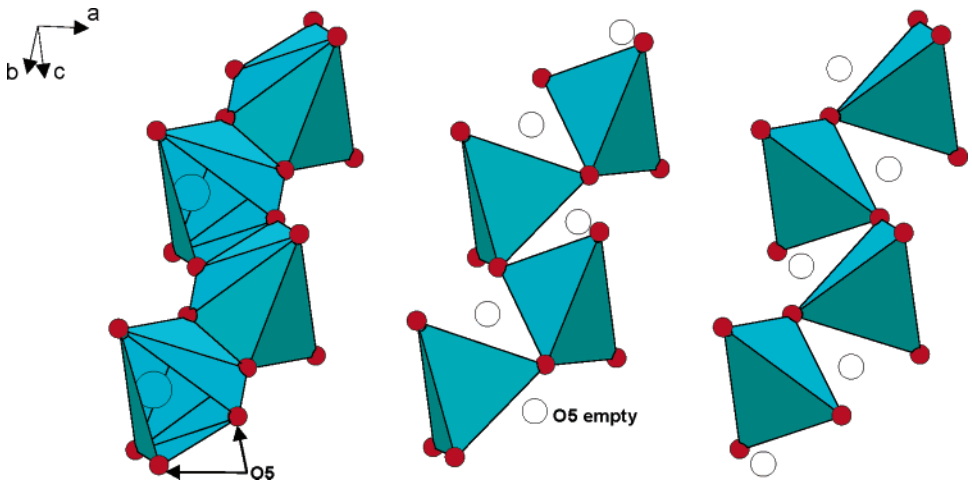

Figure 5. Distribution of the partially occupied O5 atom sites and two limit distributions leading to chains of FeO_4 tetrahedra along the *b* axis similar to those observed in the brownmillerite-type structure.

Table 4. Bond Valence Summations for All Atoms in $Sr_3NdFe_3O_9$

atom	Sr1	Sr2	Fe1	Fe2	O1	O2	O3	O4	O5
bond valence sum	1.94(3)	2.09(3)	2.97(3)	3.18(8)	1.90(2)	1.85(2)	1.39(2)	1.61(4)	1.66(7)

of +3 deduced from the stoichiometric formula $Sr_3NdFe_3O_9$.

The Sr2/Nd2 atom types that sit between the octahedral and the tetrahedral sheets are surrounded by eight oxygen atoms (Figure 4) with six short Sr2−O bonds ranging from 2.483 to 2.593 Å and two long Sr2−O4 distances of 2.819 Å. The other Sr1/Nd1 atom types present an oxygen square base pyramidal environment with all capped triangular faces. The Sr1−O distances vary from 2.397 to 2.838 Å.

^{57}Fe Mössbauer Study. The Mössbauer spectra of the as-synthesized (RP) compound registered at 273 K are shown in Figure 6. We have fitted both spectra by the presence of

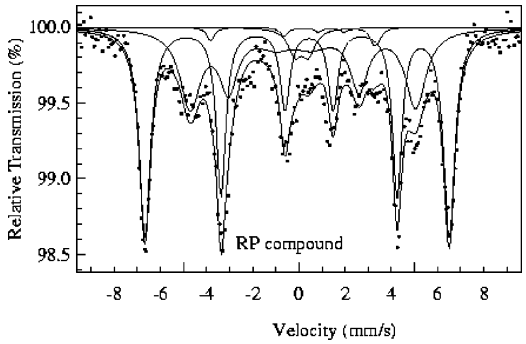

Figure 6. Mössbauer spectra of $Sr_3NdFe_3O_9$ registered at 293 K.

several iron Mössbauer components. The fitting values of the hyperfine parameters obtained by the better fit are given in Table 5. For the $Sr_3NdFe_3O_9$ compound, the results show that about 4% of iron ions are in the superparamagnetic state (D site) with the isomer shift value (IS = 0.23 mm/s) typical for Fe^{3+}. Of the iron ions in the structure, 96% are magnetic; this magnetic part consists of three different Mössbauer iron components (Table 5). The iron ions in the A site (56%; IS = 0.29 mm/s) are clearly trivalent. The high IS value (IS = 0.66 mm/s) of the smallest C component (2%) leads to the 2+ valence charge for this iron site, while the nature of the B site (38%, IS = 0.09 mm/s) is more difficult to determine. Indeed, its rather small positive isomer shift value suggests either the presence of Fe^{4+} or of Fe^{3+} with a pyramidal or tetrahedral coordination. In agreement with the neutron diffraction study, we can attribute the B component to the presence of Fe^{3+}, since no Fe^{4+} can be involved in the O_9 formula. Moreover the small IS value (0.09 mm/s) of this B component is very close to that observed for the tetrahedral Fe^{3+} species (0.11 mm/s) in Na_5FeO_4. These observations suggest that the B site of our phase corresponds mainly to Fe^{3+} in the tetrahedral environment. Thus, the fitted Mössbauer results lead to a total oxygen content equal to 8.97, very close to that observed by neutron diffraction.

Table 5. Iron Mössbauer Components of $Sr_3NdFe_3O_9$: Fitting Values of the Hyperfine Parameters[a]

RP compd	IS ± 0.02 mm/s	2ϵ* ± 0.02 mm/s	H_f ± 0.02 T	% ± 2	iron charge
A	0.29	−0.52	40.9	56	3+
B	0.09	0.40	30.3	38	3+
C	0.66	−1.7	21.9	2	2+
D	0.23	0.6		4	3+

[a] 2ϵ, quadripole shift; *, quadripole splitting of the paramagnetic component; Hf, hyper fine field; %, relative intensity.

In conclusion, this structural study of the ferrite $Sr_3NdFe_3O_9$ shows for the first time the possibility of vacancies ordering in oxygen-deficient RP-type ferrites, leading to a regular intergrowth between brownmillerite layers with K_2NiF_4-type layers. It is quite remarkable that such an oxide is very reactive with atmospheric water in contrast to the brownmillerite itself, $Sr_2Fe_2O_5$. This strongly suggests that the rock salt layers play the role of acceptors for a part of OH groups and H_2O molecules in the oxyhydroxide $Sr_3NdFe_3O_{7.5}(OH)_2 \cdot H_2O$ previously synthesized.[6] Finally, $Sr_3NdFe_3O_9$ can be considered as the first member of a series of intergrowths $(Sr_2Fe_2O_5)_n$ $SrNdFeO_4$ that should be synthesized in the future.

Supporting Information Available: Information for $Fe_3Nd_1O_9Sr_3$ (CIF). This material is available free of charge via the Internet at http://pubs.acs.org.

CM051729F

(12) (a) Hull, A. W. *Phys. Rev.* **1917**, *10*, 661. (b) Hull, A. W. *Z. Phys. Chem. (Leipzig)* **1921**, *98*, 181−210. (c) Hull, A. W. *Phys. Rev.* **1925**, *26*, 60.
(13) Bertaut, E. F.; Blum, P.; Sagnieres, A. *Acta Crystallogr.* **1959**, *12*, 149.
(14) Brown, I. D. *J. Appl. Crystallogr.* **1996**, *29*, 479.